Article:

Hewitt, D.A. orcid.org/0000-0002-4585-2915, Sundeep, S. orcid.org/0000-0001-7278-7613, Griffo, A. orcid.org/0000-0001-5642-2921 et al. (1 more author) (2024) Impact of close proximity pulse width modulation switching events on electric machine terminal voltages. IET Electric Power Applications, 18 (11). pp. 1458-1468. ISSN 1751-8660

https://doi.org/10.1049/elp2.12495

Received: 17 June 2024 | Revised: 18 August 2024 | Accepted: 9 September 2024

DOI: 10.1049/elp2.12495

IET Electric Power Applications

The Institution of Engineering and Technology WILEY

ORIGINAL RESEARCH

Impact of close proximity pulse width modulation switching events on electric machine terminal voltages

David A. Hewitt[1] | Shubham Sundeep[1,2] | Antonio Griffo[1] | Jiabin Wang[1]

[1]Department of Electronic and Electrical Engineering, University of Sheffield, Sheffield, UK

[2]National Renewable Energy Laboratory, Arvada, Colorado, USA

Correspondence

David A. Hewitt.
Email: david.hewitt@sheffield.ac.uk

Funding information

Engineering and Physical Sciences Research Council, Grant/Award Number: EP/S00081X/1; UK Research and Innovation

Abstract

Electric machines form an essential part of a wide range of modern systems. When speed control is required, the use of pulse width modulation-based inverters is generally the solution of choice. It is also usual to connect the machine to the inverter using a cable. The combination of these three elements produces the potential for voltages which exceed the dc link voltage to occur at the machine terminals. Methods for predicting the terminal voltage exist; however, these methods assume that the pulses applied to the system can be considered as isolated, discrete events. The authors highlight an issue with this assumption. When a switching event occurs, it will cause a voltage disturbance in the unswitched phases of the system due to the mutual coupling between the phases. If a second switching event occurs within a short time of this event the resultant voltage will interact with the previous switching event resulting in a higher terminal voltage than would be the case for an isolated event. This effect can be problematic for insulation design if it is not considered. This issue is demonstrated, with the worst-case scenarios identified and potential methods of reducing terminal voltage being proposed.

KEYWORDS

electric machines, electromagnetic coupling, insulation, pulse width modulation

1 | INTRODUCTION

Electric machines are essential components in a wide range of applications. A common topology employed in machine design is the 3-phase star-connected machine. To produce rotation, the three phases are driven by three sinusoidal currents which are electrically displaced from each other by 120°. In applications requiring speed and/or torque control, pulse width modulation (PWM)-based inverters are usually employed. These inverters generate an approximation of the sinusoidal currents through the coordinated switching of multiple switching elements (e.g. MOSFETS or IGBTs). This approach produces a train of pulses which, when applied to the winding inductance, average to produce an approximation of the required sinusoidal waveform. To reduce the level of distortion in this current waveform the PWM switching frequency should be substantially higher than the fundamental rotation frequency of the machine (usually of the order of kHz).

To reduce the switching losses which occur within the inverter, it is advantageous for the switching events to occupy possibly a short time period by employing fast rise and fall times. The development of newer wide-bandgap technologies, such as SiC and GaN offer the potential for higher power densities through the facilitation of faster rise times and higher switching frequencies, allowing these values to be pushed to levels which would not be practical with conventional Si-based devices [1–3]. These factors, coupled with the increasing trend to use higher DC-link voltages in many applications such as electric vehicles result in high rates of dV/dt being applied to the machines.

In a practical system, the machine will be connected to the inverter using a cable. Due to impedance mismatches between the machine and cable, voltage overshooting at the machine terminals will occur [4]. Research has shown that for cables shorter than the critical length (that is cables for which the propagation time is less than the converter rise time) overshoot

Shubham Sundeep is formally at University of Sheffield.

voltage magnitude is inversely proportional to rise time—that is to say that faster rise times will result in a greater level of overshoot [4–6].

Voltage overshoot can cause a range of issues for an electric machine. Most obviously, if the overshooting voltage exceeds the breakdown voltage of the insulation, failure will occur. Less obviously, but potentially just as harmful, is the condition where voltage exceeds the partial discharge inception voltage (PDIV) of the insulation. In this case, total insulation failure will not occur immediately; however, discharges will occur within the air voids of the insulation, which over time will result in insulation degradation leading to premature failure [7]. Consequently, a good understanding of the voltages which occur at machine terminals is vital for the understanding of machine lifetimes.

Methods for predicting the overshoot voltage for a given system already exist in the literature [5, 8, 9]. One such method which will be discussed here is described in ref. [5]. It is assumed in all these methods that each switching event can be treated as a discreet event and can be considered in isolation. When this condition is true, these methods can predict the overshooting voltage with a reasonable degree of accuracy; however, in cases which this condition is not true, for example, when multiple phase transitions occur within a short period of time, the interaction between these events can result in overshooting voltages which are substantially higher than would be predicted using this method.

It has been reported in literature [6, 8, 9] that terminal voltage stress may be increased if a single phase is switched for a second time while oscillation is still present from the first switching event. In this article, it is demonstrated that such interactions can also occur between the phases if the switching events occur on different phases, due to the mutual inductance between the phases. While some more recent models which incorporate the mutual inductance between phases do exist in literature, for example, in refs. [10–13] the impact of different phases switching within a short time frame, and the resultant impact on terminal jump voltages is not explicitly discussed in these cases. This phenomenon, which has not been widely reported, is the primary focus of this paper. In addition to this, a method of obtaining the parameters for the overshooting prediction model based on common-mode impedance measurements of the system under test is also presented. An empirical model of the system under study which includes the impact of phase interactions is also employed to identify the worst-case inverter operating points with respect to terminal voltage.

2 | STUDIED SYSTEM CONFIGURATION

A typical configuration for a PWM driven machine is shown in Figure 1. This system consists of a PWM inverter which is supplied by a dc link voltage (V_{dc}). This generates the PWM waveforms used to drive the machine. Connection between the inverter and machine is achieved using a length of shielded cable. Here each conductor is individually insulated, and the entire cable is shielded using a common shield. If grounding is required, this shield is connected to the midpoint of the dc link voltage at the inverter end and to the machine casing at the machine end. In some configurations, a separate protective earthing connection is required, in such cases a fourth conductor may also be included for this purpose. The configuration shown in Figure 1 is a generalisation, and other shielding/protective earthing arrangements may be required for specific applications. Such discussion is application specific and beyond the scope of this article as it will not significantly impact the key phenomenon under discussion. In the example considered here the machine is connected in star configuration, this is a typical configuration for machines of this type. In the work discussed here, the voltages referred to as the machine terminal voltages are measured at the point between the end of the cable and the machine terminals. The machine casing voltage is used as the reference point for these measurements.

In the presence of rapidly changing waveforms, for example, PWM signals with fast rise times, wave propagation effects can influence the voltage which is present at the machine terminals. When a switching event occurs, this waveform will propagate along the connecting cables, and through the machine windings. Due to impedance mismatches at the interface between the cable and windings, reflections will occur at the machine terminals. These reflections interact with the incoming signal, resulting in higher voltages being observed at the machine terminals [5].

To study these effects in this article an example system is employed. The specifications of the machine used for this study are listed in Table 1. In this study, the test sample consisted of a machine stator only (no rotor), this will not have a significant impact on the observations made in this work but simplifies the experimental setup considerably. A photograph of the stator is shown in Figure 2. PWM signals are generated in this work using a SiC-based 2-level PWM inverter and connections between the stator and inverter are made using a

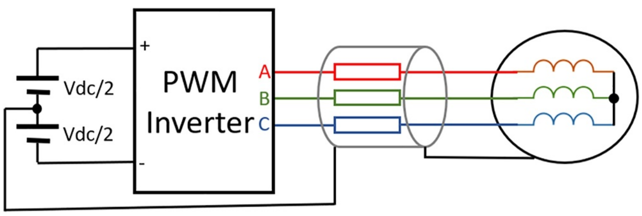

FIGURE 1 Configuration of typical PWM drive driven system.

TABLE 1 Machine specifications.

Parameter	Value
Type	Permanent magnet servo motor
Phases	3
Winding type	Distributed, single layer
Power rating	2.8 kW

2.5 m long shielded cable. This experimental setup is shown in Figure 3, an oven is employed as an enclosure for the sample under test to protect the operator from exposure to high voltages, during this testing the oven was not turned on and was not used to heat the sample.

3 | PREDICTION OF VOLTAGE OVERSHOOT

The underlying method discussed here for the prediction of voltage overshooting was first proposed in ref. [5]. In this section, the relevant equations will be briefly summarised, along with a newly proposed alternative method of characterising the parameters for an electric machine system, based on common mode impedance measurements of the cable and machine.

Ultimately, the parameter which is of interest when predicting the level of voltage overshoot is the reflection coefficient Γ, which can be calculated using Equation (1).

$$\Gamma = \frac{Z_m - Z_c}{Z_m + Z_c} \tag{1}$$

FIGURE 2 Stator sample under test.

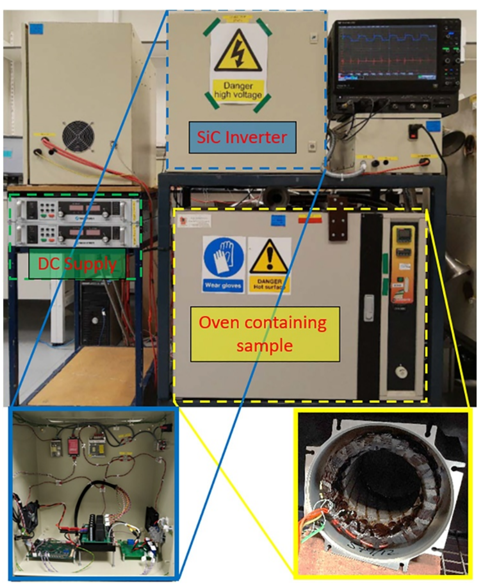

FIGURE 3 Experimental setup used for this study.

Where Z_m and Z_c are the surge impedance values of the machine and cable respectively. The surge impedance of an element can be calculated as follows:

$$Z_c = \sqrt{\frac{L_C}{C_c}}, Z_m = \sqrt{\frac{L_m}{C_m}}, \tag{2}$$

Where L_c and L_m represent the per unit inductance of the cable and machine respectively, and C_c and C_m represent the per unit cable and machine capacitance values.

While it is possible to calculate the surge impedance of a component by measuring the L and C values, an alternative approach using measurements of the common mode impedance can be employed. By way of example, the common mode impedance of the cable studied in this work is shown in Figure 4. From this data, two parameters can be determined. Firstly, the capacitance is extracted from the impedance data, this is done at a low frequency (10 kHz) as at this frequency the impedance angle can be observed to be very close to −90°, meaning that the impedance is predominantly capacitive at this frequency. The second extracted parameter is the first anti-resonant frequency of the cable. These values can be used to calculate the surge impedance of the cable using equations (3)–(7).

The propagation time of the cable is given by the following [5]:

$$t_{p(cable)} = \frac{l_c}{v} = l_c \sqrt{L_c C_c} \tag{3}$$

Where $t_{p(cable)}$ is the propagation time of the cable, l_c is the length of the cable, and v is the velocity at which the pulse propagates through the cable.

The relationship between the first anti-resonant frequency and the propagation delay is shown in Equation (4) [10]. By rearranging Equation (4) and substituting it into Equation (2) it

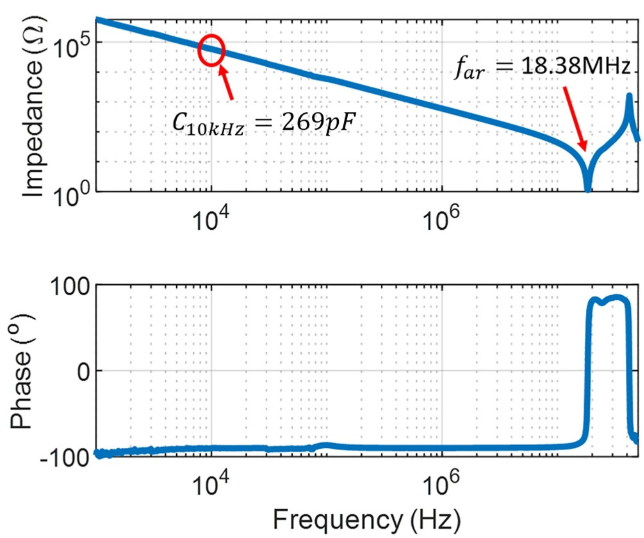

FIGURE 4 Measured common mode impedance of cable.

is possible to obtain Equation (5). As the cable common mode capacitance (C_{CCM}) is equal to the product of the cable length, and the per unit capacitance (6) the final equation for cable surge impedance (7) can be obtained.

$$f_{ar} = \frac{1}{4t_{p(cable)}} = \frac{1}{4l_c\sqrt{L_c C_c}} \tag{4}$$

$$Z_c = \frac{1}{4f_{ar}l_c\sqrt{C_c}}\frac{1}{\sqrt{C_C}} = \frac{1}{4f_{ar}l_c C_c} \tag{5}$$

$$C_{CCM} = C_c l_c \tag{6}$$

$$Z_c = \frac{1}{4f_{ar}C_{CCM}} \tag{7}$$

This approach may not be necessary for the cable, as it is relatively trivial to determine the cable length through measurement, allowing the use of Equation (2) directly. However, this equation can also be applied to the machine surge impedance by replacing the cable parameters with parameters for the machine. This is helpful as determining the length of the machine windings is much more difficult given their wound arrangement.

The common mode impedance of the cable and machine were each measured using Bode 100 vector network analyser in the configuration shown in Figure 5. Using equations (1)–(7) combined with the data presented in Figures 4 and 6 the values for the system under study can be calculated. These values are listed in Table 2.

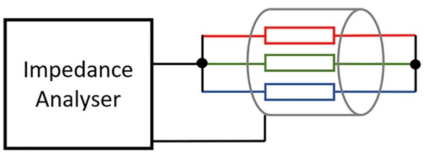

FIGURE 5 Measurement setup used to measure common mode cabled impedance.

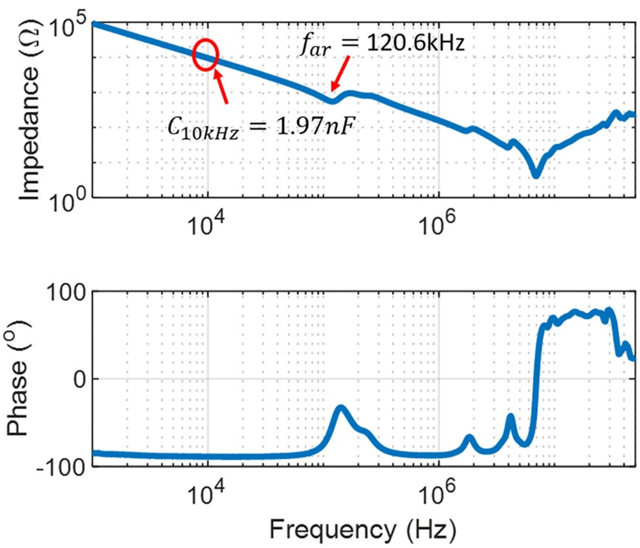

FIGURE 6 Measured common mode impedance of machine.

Calculating the expected terminal overshooting value from the reflection coefficient can be achieved using Equations (8) or (9) [5]. The correct equation in this instance depends on the propagation time relative to the signal rise time [5]. In this article, a nominal rise time of 60 ns is considered. In this case, three times the cable propagation delay (3 × 13.6 ns) is less than the rise time, therefore the correct equation is (8). Using this equation for the converter rise times yields a predicted terminal overshooting value of 1.62, which equates to a voltage of 162 V when a 100 V dc link is used.

$$\frac{V_{t_{max}}}{V_{DC}} = 1 + \frac{3t_{p(cable)} * \Gamma}{t_r} \qquad \text{If } 3t_{p(cable)} < t_r \tag{8}$$

$$\frac{V_{t_{max}}}{V_{DC}} = 1 + \Gamma \qquad \text{If } 3t_{p(cable)} \geq t_r \tag{9}$$

Where $V_{t_{max}}$ is the peak terminal jump voltage, V_{DC} is the dc link voltage and t_r is the converter rise (or fall) time.

4 | EXPERIMENTAL RESULTS

Testing was performed using a dc link voltage of 100 V. The converter was operated in open loop mode with a modulation index value of 0.5. The inverter was configured to provide a nominal rise time of 60 ns with a 40 kHz switching frequency and the fundamental frequency of the drive was set to 200 Hz. The captured machine terminal voltages measured relative to the machine casing are shown in Figure 7. The captured data here shows over 120° of the electrical cycle, which due to the symmetry of the system, is sufficient to illustrate the behaviour over the entire cycle, as the behaviour will repeat, with the position of the phases swapped. This will not impact the behaviour being discussed here.

Over the course of the electric cycle, it can be observed that the peak terminal voltage values are not consistent. The reasons for this will be discussed in the following section.

4.1 | Impact of phase interaction

Consider the case shown in Figure 8. This data shows an extract from Figure 7 in which of the switching events within

TABLE 2 Calculated values for setup under test.

Parameter	Value
Z_c	50.56 Ω
$t_{p(cable)}$	13.6 ns
Z_m	1052.27 Ω
Γ	0.908

the PWM cycle are spread out and each phase switching event can be considered in isolation. The first thing to observe is that whenever a switching event occurs a corresponding disturbance is also visible in the other phases. This disturbance can be attributed to the mutual inductance between the phases, both in the machine and the cable. When a rapid change in current (for example a switching event) occurs, this will excite the mutual inductance between the phases, resulting in a voltage being induced in the other phases. The presence of high frequency components within these coupled signals supports the explanation that they are caused by magnetic coupling rather than the signal propagation through the windings. Considering the results presented in ref. [11] it can be observed that as the signal propagates through the windings, the winding behaves as a low pass filter, removing the high frequency elements from the signal. The oscillations observed on the unswitched phases contain frequency components which match the high frequency oscillation of the switched phase, suggesting that these signals have not propagated through the winding, as high frequency components of this magnitude cannot be observed at the neutral point of the machine.

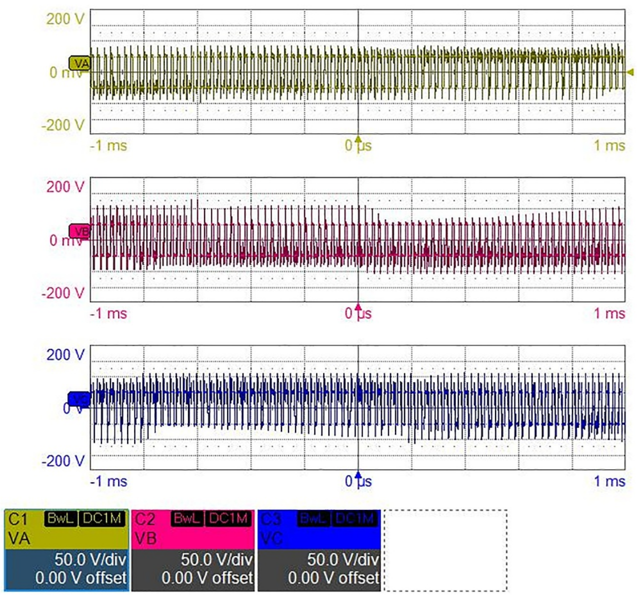

FIGURE 7 Sample terminal voltage measurements (Vdc = 100 V, m = 0.5, tr = 60 ns).

In cases such as the one shown in Figure 8, the disturbances do not substantially impact the observed terminal jump voltage, as the disturbance has time to decay before the next pulse is applied. Consequently, the voltages observed in phases B and C are very close to the predicted values using the method discussed in the previous section. The lower value observed in phase A can be explained by several factors including discrepancies in rise time and imbalances between the machine phases.

The discrepancy between nominal and actual rise times can be attributed to a combination of factors. Firstly, component tolerances will cause each phase leg to switch at slightly different speeds. Secondly, at different points in the electrical cycle, the polarity and magnitude of the load current will vary. This current interacts with the parasitic capacitances of the MOSFET resulting in differences in rise time. A detailed discussion of this behaviour is studied in ref. [14].

A further extract from the data is shown in Figure 9. Similar to the previous example, phase C switches in isolation from the other phases; consequently, there are no disturbances from other phases influencing this switching event. In this case, the magnitude of the jump voltage is very similar to the previous example (2 V difference). The slight difference which

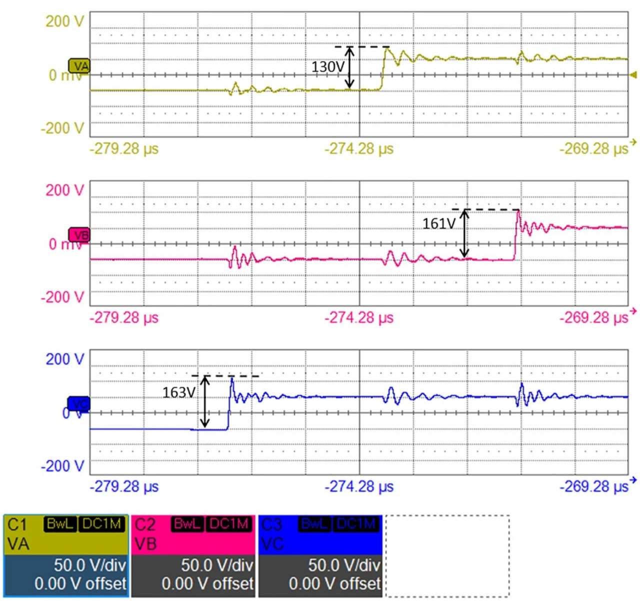

FIGURE 8 Zoomed view of a single PWM switching set extracted from Figure 7 showing widely spaced switching (Measured).

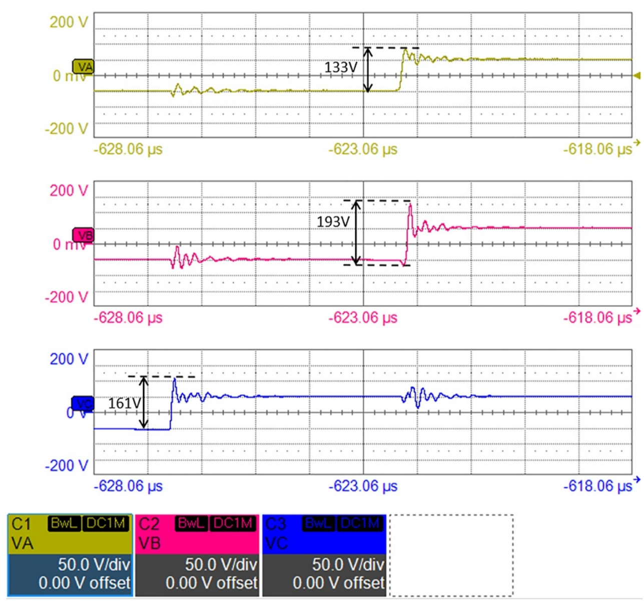

FIGURE 9 Zoomed view of a single PWM cycle extracted from Figure 7 showing close switching (Measured).

is observed between the examples can be attributed to differences in the electrical angle and by extension the load current, which will result in slight differences to the converter rise time [14].

Unlike the previous example, in this case phase A and phase B switch within a very short time period. The impact of this can be observed by considering phase B. Initially, the disturbance induced by the switching of phase A causes the voltage of phase B to decrease; while this voltage is lower than the resting value, the phase B rising edge occurs. Consequently, the resulting jump voltage consists of a combination of the rising edge and the previous disturbance, resulting in a jump voltage which is substantially higher than the previous case (~20%).

This demonstration illustrates the reason for the observed variations in measured terminal voltage over the course of an electrical cycle. It also highlights that the conditions under which larger than predicted overshoots can occur exist even at relatively high modulation index values. By inspection of the PWM switching sequence it can be observed that, these conditions will occur whenever the electrical angle of the inverter space vector voltage is close to integer multiples of 60 electrical degrees. In such cases, two phases will switch within a short time. It is also possible for all three phases to switch in close proximity; however, this will only occur when the modulation index is low.

To illustrate this, the converter was operated using a modulation index value of 0.01. A sample switching event from this test is shown in Figure 10. In this example, phases A and B switch simultaneously, and phase C switches shortly afterwards. The most significant impact of this can be observed in phase C. Once again, the disturbances caused by the switching of the other phases results in a decrease in voltage prior to switching, causing the overall jump voltage to

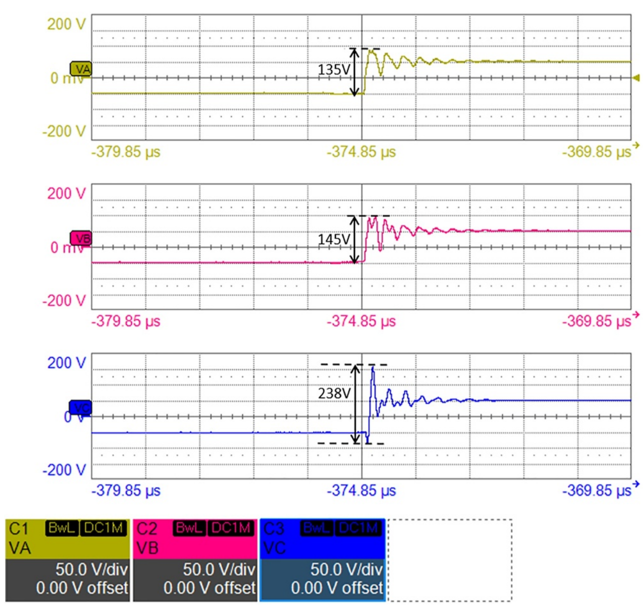

FIGURE 10 Zoomed sample terminal voltage measurements, all three phases close switching (Vdc = 100 V, m = 0.01, tr = 60 ns) (Measured).

increase. Another interesting observation in this case is the behaviour of phase B, in this case the value is slightly reduced compared to the isolated switching case. Here the interaction between the phases results in the peak of the waveform coinciding with the trough of the mutually inductance voltage, the superposition of these two signals results in a net decrease in the terminal voltage. While such an occurrence is possible, it should not be relied upon as a means of reducing the terminal voltage, as such behaviour will not occur consistently throughout the electrical cycle.

These results demonstrate that although the analytical method discussed in section 3 is a valuable tool for obtaining an indication of the likely voltage levels, it is not fully adequate for predicting voltages if multiple phases are likely to switch near each other. While this is more of an issue when inverters are operated at lower modulation index values it has also been shown here that even at higher values of modulation, this phenomenon will still occur when the electrical angle of the space vector voltage approaches integer multiples of 60 electrical degrees.

5 | ANALYTICAL ANALYSIS

The previously presented results demonstrate the phenomena under discussion and its impact on the voltages experienced at the machine terminals. To further study this effect, it is helpful to consider the overall impact of modulation index and electrical angle on the terminal overshoot value. While this could be achieved by performing many experimental tests, it is preferable to be able to perform this analysis analytically. To this end a model is generated to characterise the system under test based on a limited number of experimental data points. This approach allows the entire experimental space to be considered without the need for many experimental tests. In this section such a model is discussed, culminating in the production of a surface which comprehensively explores the relationship which exists between modulation index, electrical angle, and terminal jump voltage.

The model employed for this purpose is based on travelling wave theory which is discussed in general terms in ref. [15], the specific derivation as applied to an electric machine problem is also discussed in ref. [11] and is built on the time domain second order step response of the system. As it is necessary to consider the interaction of multiple switching events it is necessary to use a version of this model which allows for non-zero initial conditions. In this implementation of the model the input signal is the inverter output. The model captures the behaviour of the signal propagation through the cables and machine windings, allowing the model to be used to calculate the voltages at the machine terminals in this system.

To use this model, first the terminal voltage contribution from each phase is calculated using Equation (10). This equation determines the oscillating component contribution to the terminal voltage. In addition to these oscillations, the dc contribution to the signal caused by the switching action of the inverter must also be included for the phase under study. This is calculated using Equation (11). These voltages can then be combined using Equation (12) to obtain the total terminal voltage for a phase. Since the coupling between the phases is caused by magnetic coupling, only signals with an AC component will be transferred. Consequently, as can be seen in Equation (12), only the DC component of the phase under study is considered. In the case of the phase under study, the value of V_{x_m} is empirically determined such that the peak oscillation value matches the experimental peak value in the data used to calibrate the model. The magnitude of this value will be impacted by properties of the system such as the rise time and cable propagation time, as discussed previously. In the case of the coupled phases V_{x_m} is impacted by both the magnitude of the switching oscillations, and level of coupling between the phases. Again, this value is determined empirically, such that the magnitude of the modelled oscillations which occur in the unswitched phases during an isolated switching event match the experimentally observed values.

$$\begin{aligned} V_{X_{AC}} = V_{X_m}\sqrt{1+\left(\frac{\xi}{\omega}\right)^2}\mathrm{e}^{-\xi(t-\tau_X)}\sin\Bigg(\omega(\mathrm{t}-\tau_{\mathrm{X}}) \\ +\tan^{-1}\left(\frac{\xi}{\omega}\right)-\frac{\pi}{2}\Bigg) \\ +V_{X_0}\sqrt{1+\left(\frac{\xi}{\omega}\right)^2}\mathrm{e}^{-\xi(\mathrm{t}-\tau_{\mathrm{X}})}\sin\Bigg(\omega(\mathrm{t}-\tau_{\mathrm{X}}) \\ +\tan^{-1}\left(\frac{\xi}{\omega}\right)+\phi_{X_0}-\frac{\pi}{2}\Bigg) \end{aligned} \tag{10}$$

Where $V_{X_{AC}}$ represents the ac component of a phase ($X = A, B, C$), V_{x_m} is the initial amplitude of the phase voltage oscillation, ξ is the damping factor, ω is the damped frequency of oscillation, τ_X is the time at which the switching event occurs in phase X and V_{X0} and ϕ_{X_0} represent the initial magnitude and phase of the damped sinusoidal oscillation. On model initialisation the initial values will be zero, however, when successive switching events occur the values will be updated in accordance with the procedure illustrated in Figure 11, allowing the initial conditions at successive switching events to be captured.

$$V_{X_{DC}} = \frac{V_{DC}}{2} \qquad \text{If } S_X \text{ is high} \tag{11}$$

$$V_{X_{DC}} = -\frac{V_{DC}}{2} \qquad \text{If } S_X \text{ is low}$$

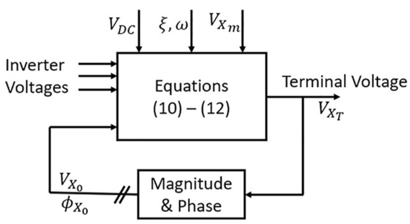

FIGURE 11 Block diagram of analytical model implementation.

Where $V_{X_{DC}}$ is the dc component of the phase under study (X), V_{DC} is the DC link voltage and S_X is the inverter switch state which is driving phase X.

$$V_{X_T} = V_{X_{DC}} + V_{X_{AC}} + V_{Y_{AC}} + V_{Z_{AC}} \tag{12}$$

Where V_{XT} is the voltage at the terminal under study, X is the phase under study, and Y and Z are the remaining phases, such that $X \neq Y \neq Z$.

The values of ξ and ω are calculated using the measurements illustrated in Figure 12 and Equation (13).

$$\xi = \frac{\ln(\mathrm{V}_2) - \ln(\mathrm{V}_1)}{\mathrm{t}_2 - \mathrm{t}_1} \tag{13}$$

The parameterisation of this model requires prior knowledge of the system behaviour to allow suitable tuning to be performed. In this example, the model is tuned using experimental data, after which the model is used to extensively explore the experimental space without the need for additional experimentation to be performed. As an alternative to using experimental data, this model could be tuned using data from a high frequency model, for example, the model discussed in ref. [11]. Due to the complexity of such high frequency models, it is difficult to explore a wide range of operating points using such a model directly, due to the long time required to solve the high-fidelity model. Using the simpler analytical approach allows the terminal behaviour of the machine to be replicated using a considerably simpler model, facilitating a much wider analysis of operating points at reduced computational expense.

To evaluate the performance of this model against the experimental data two comparisons are presented here. Firstly, the example period initially discussed in Figure 8 is shown in Figure 13. In this example, all three phases are switched in

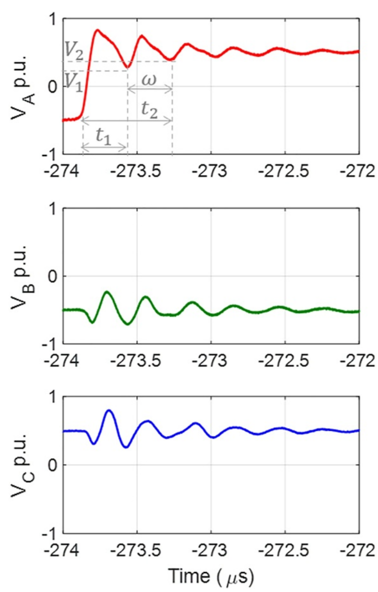

FIGURE 12 Experimental determination of damping factor (ξ) and oscillation frequency (ω).

isolation. Comparing the measured and predicted terminal voltage in this case it can be observed that the peak voltage values of both the switching event and coupled disturbances caused by the switching of other phases match well. Similarly, the case demonstrated in Figure 14 was originally presented in Figure 9 and provides an example of multiple switching events occurring in proximity. Again, in this case the peak voltage values are well represented, as are the interactions between the phases. In both cases, the peak values match well, it should be noted that there are differences between the precise shape of the waveforms owing to higher order harmonics being included in the measured data which are not included in the model. As the main objective of this model is to predict the peak terminal jump voltage, this is not detrimental to this objective.

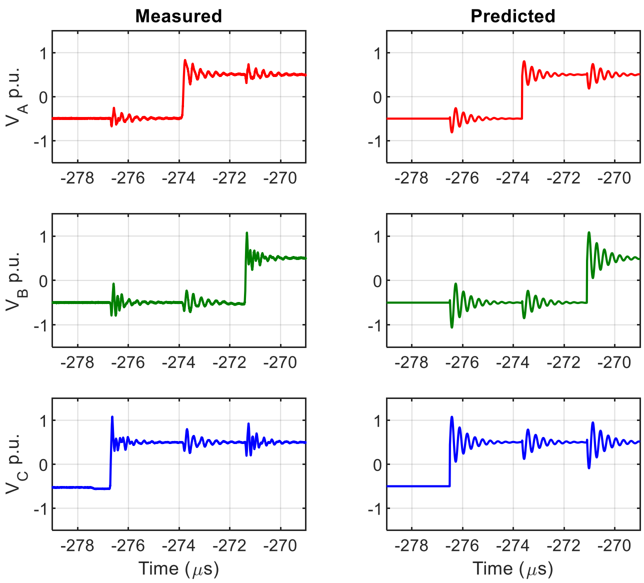

FIGURE 13 Example comparison of measured and predicted terminal voltages for isolated switching events.

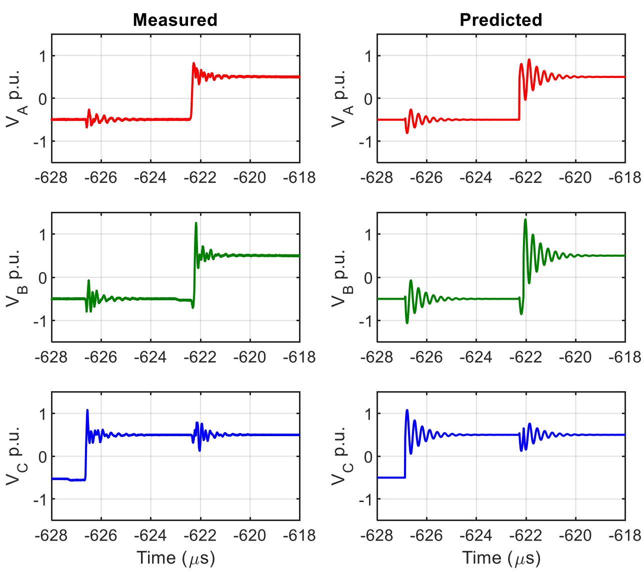

FIGURE 14 Comparison of measured and predicted terminal voltages for overlapping switching events.

Simulating the model for a comprehensive range of modulation index and electrical angle values allows the impact of these variables to be explored fully. This approach allows the impact of these variables to be assessed, and to confirm the observations made previously based on the experimental data. The relationship between these variables is shown in Figure 15 for phase A. Similar analysis was also performed for the other phases, but as the conclusions are consistent across the phases, only phase A will be discussed here for brevity.

Considering the results presented in Figure 15 a few important observations can be made. Firstly, regardless of modulation index value, pronounced peaks in jump voltage can be observed at regular intervals with respect to electrical angle. These peaks in jump voltage value occur at 60° increments and coincide with changes in the space vector sector. At these points, switching of two phases will occur in close succession, this will occur regardless of modulation index value, leading to an increase in jump voltage in all cases. It is also interesting to note that in the case of phase A, peak values occur consistently due to this effect at 60°, 120°, 240° and 300°. This is to be expected, as considering the state vectors at these points phase A will switch simultaneously with another state. In the cases of 0° and 180°, phase A will switch in isolation, and phases B and C will switch together. This results in the jump voltage at these angles being comparable to the isolated switching value, which for phase A has been shown to be ~1.3 p.u.

Additionally, at low modulation index it can be observed that the jump voltage is further increased. This can be attributed to the fact that at low modulation index values all three phases will switch within a short time, resulting in interaction between the three phases and resulting in a further increased jump voltage. This differs from the case observed at higher modulation index values, where only a maximum two phases will switch closely enough to cause significant interactions between the switching events. From this it can be concluded that the worst case for terminal voltage stress will occur at low values of modulation index. It should be noted however that

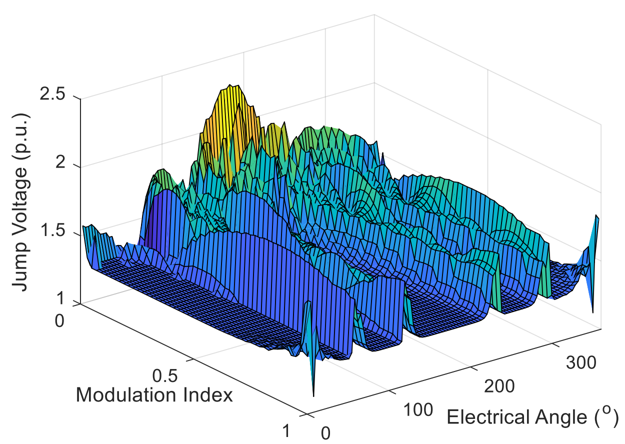

FIGURE 15 Surface showing predicted terminal jump voltages with respect to modulation index and electrical angle (phase A).

the electrical angle will also have some impact in the terminal jump voltage, meaning that it cannot be assumed to be constant over an electrical cycle regardless of modulation index value.

To verify the trends predicted by the model the jump voltage over 60 electrical degrees is evaluated from experimental data under two different modulation index values. The first case considered is when the modulation index value is 0.5. The jump voltages for all three-phases are shown in Figure 16. For some of the sector shown here phases A and B switch close together, over the entire sector, phase C will switch in isolation. Firstly, considering phase C, the value is stable across the time period considered, and is consistent with the values discussed in the earlier analysis (~1.65). The impacts of phase A and B on each other can be clearly seen by the increases in jump voltage observed in both phases. This observation corroborates the behaviour exhibited by the model and confirms the observed trends in this case. In the second half of the data shown in this figure, all three phases are switched in isolation, yielding jump voltages comparable to the previously observed individual cases.

Further analysis is also performed, considering experimental data with a modulation index value of 0.01. This data is presented in Figure 17. Here the results shown for phase C exceed any values shown in higher modulation/isolated switching case. Also, due to the very short window occupied by all three switching events the jump voltage values for this phase are higher than the isolated case across the entire period shown.

It has also been discussed previously, that in some cases the interference between the phases can result in a decrease in the jump voltage, this behaviour can be seen in phase B in this case, where in some instances the jump voltage value is below the typical isolated switching value observed previously of ~1.6. Overall, the trends observed in the experimental data are consistent with the behaviour predicted by the model regarding phase interactions and the impact they will have on jump voltages.

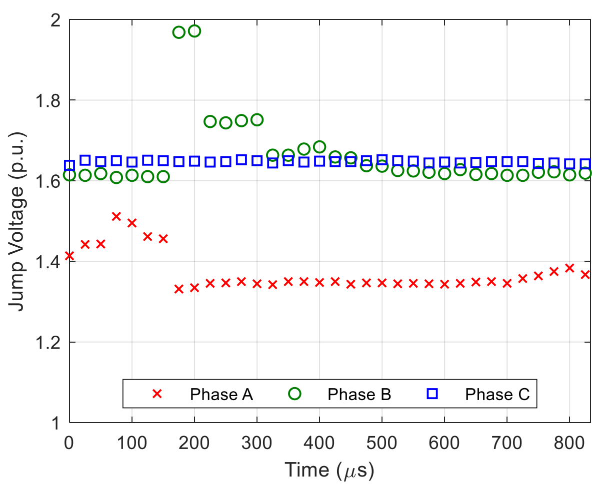

FIGURE 16 Experimental jump voltage of phases over 1/6 of an electrical cycle ($m = 0.5$).

The discussion above has focused on the voltages which appear at the machine terminals; however, due to signal propagation effects the observed increase in voltages will also impact the turn-to-turn voltages within the windings. The measurement of these voltages is much more challenging as to do so requires machine disassembly/the production of a modified stator which incorporates winding taps. Theoretically it is possible to apply this model to the prediction of voltages within the winding, however due to limitations in the acquisition of calibration data this would be more challenging than the currently presented terminal voltage case. In the absence of suitable calibration data it may be more suitable to consider a high frequency model which is suitable for parameterisation using finite element data directly, for example ref. [16]; however, such models tend to be substantially more complex than the approach discussed here owing the level of fidelity required to accurately capture the behaviour throughout the winding. Such complexity is potentially necessary if knowledge of the turn-to-turn voltages within the machine is required.

It is also worth noting that studies which consider the behaviour of the propagating waves thought the windings [10, 17] show that the high frequency signals which are associated with switching events do not propagate through the entire winding due to the inductive nature of the windings. Studies also show that the peak voltages within the windings (measured relative to the stator core) occur at the machine phase terminals, and at the neutral point making these the most important locations to consider.

6 | REDUCTION OF TERMINAL VOLTAGE LEVELS

While the primary focus of this paper is highlighting the significant contribution which phase interactions can have on machine terminal voltage, it may be helpful for designers to consider potential methods of reducing the terminal voltage. This section is included for this purpose.

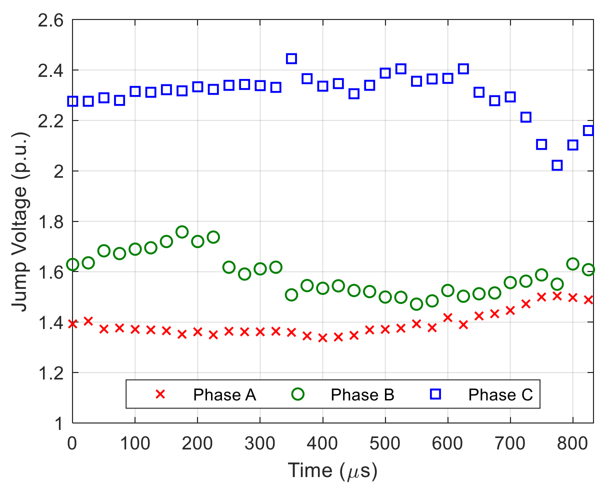

FIGURE 17 Experimental jump voltage of phases over 1/6 of an electrical cycle ($m = 0.01$).

Firstly, the use of shorter cables may reduce the level of overshooting observed at the machine terminals, this can be observed by inspection of Equation (8), as a shorter cable will have a lower propagation time, resulting in a lower overshooting value. It is also important to ensure that the cables are shorter than the critical length to prevent pulse doubling effects from occurring [6].

Another potential approach is to reduce the level of magnetic coupling between the phases, this could be achieved by using individually shielded cables, or choosing a machine design which exhibits lower levels of inter-phase mutual inductance, for example, by employing single layer windings [18–20]. Depending on the application such factors may be outside the control if the designer, but in cases where this is possible, consideration of these factors has the potential to result in lower insulation stresses.

It is also possible to apply constraints to the converter to reduce the terminal overshooting voltages. These include limiting/increasing the converter rise time, limiting the allowable modulation index of the converter and preventing multiple rising/falling edges from occurring at the same time. Limiting converter operation in this way can lead to waveform distortion and underutilisation of the dc link by limiting the areas of the space vector plot which can be used. Additionally, slowing down the switching of the devices may negate the advantages of employing wide bandgap devices, as the imposed limits could place the converter within the scope of silicon-based devices.

It may be also possible to add additional hardware to the system, for example, filters to reduce the terminal voltage overshooting levels [5, 21–23]; the appropriateness of such techniques will be very much dependent on the application, placing them outside the scope of this paper.

7 | CONCLUSIONS

In this article, a method for predicting the voltages which will occur at the terminals of an electric machine has been evaluated. This technique has been demonstrated to be reasonably accurate when considering applied pulses in isolation. However, experimental results demonstrate that this technique is less effective if multiple pulses occur close together and interact with each other. This finding highlights two key points which are worth considering.

Firstly, when multiple switching events occur within a short period of time, the jump voltage at the machine terminals will be higher than would be the case for pulses in isolation, this is caused by the interaction between multiple switching events, either in the same phase, or different phases via the inter-phase mutual coupling.

Secondly, methods which do not account for these effects will underestimate the potential voltage stresses which will be experienced by the machine insulation, resulting in an under-specified insulation system. This will be problematic for the lifetime of the machines in service as it will lead to overloaded insulation, and reduced lifetime.

An analytical model based on second order step response is used to comprehensively evaluate the terminal jump voltage with respect to inverter modulation index and electrical angle. From this it is concluded that the jump voltage will be at its highest when multiple switching events occur close together. Consequently, the worst-case jump voltage will occur when the modulation index is low, as in such cases, all three phases will be switched in a very short period.

AUTHOR CONTRIBUTIONS

David A. Hewitt: Data curation; formal analysis; methodology; software; visualisation; writing - original draft; writing - review & editing. **Shubham Sundeep**: Data curation; formal analysis; investigation; methodology; software; writing - review & editing. **Antonio Griffo**: Conceptualisation; funding acquisition; supervision; writing - review & editing. **Jibing Wang**: Conceptualisation; funding acquisition; supervision; writing - review & editing.

ACKNOWLEDGEMENT

This work was supported by the UKRI under Grant EP/S00081X/1.

CONFLICT OF INTEREST STATEMENT

The authors declare no conflict of interest.

DATA AVAILABILITY STATEMENT

The data that support the findings of this study are available from the corresponding author upon reasonable request.

ORCID

David A. Hewitt https://orcid.org/0000-0002-4585-2915
Shubham Sundeep https://orcid.org/0000-0001-7278-7613
Antonio Griffo https://orcid.org/0000-0001-5642-2921
Jiabin Wang https://orcid.org/0000-0003-4870-3744

REFERENCES

1. Bindra, A.: Wide-bandgap-based power devices: reshaping the power electronics landscape. IEEE Power Electronics Magazine. 2(1), 42–47 (2015). https://doi.org/10.1109/mpel.2014.2382195
2. Chow, T.P., et al.: Smart power devices and ICs using GaAs and wide and extreme bandgap semiconductors. IEEE Trans. Electron. Dev. 64(3), 856–873 (2017). https://doi.org/10.1109/ted.2017.2653759
3. Lemmon, A.N., Graves, R.C.: Comprehensive characterization of 10-kV silicon carbide half-bridge modules. IEEE Journal of Emerging and Selected Topics in Power Electronics 4(4), 1462–1473 (2016). https://doi.org/10.1109/jestpe.2016.2606120
4. Persson, E.: Transient effects in application of PWM inverters to induction motors. IEEE Trans. Ind. Appl. 28(5), 1095–1101 (1992). https://doi.org/10.1109/28.158834
5. Jouanne, A.v., Enjeti, P.N.: Design considerations for an inverter output filter to mitigate the effects of long motor leads in ASD applications. IEEE Trans. Ind. Appl. 33(5), 1138–1145 (1997). https://doi.org/10.1109/28.633789
6. Kerkman, R.J., Leggate, D., Skibinski, G.L.: Interaction of drive modulation and cable parameters on AC motor transients. IEEE Trans. Ind. Appl. 33(3), 722–731 (1997). https://doi.org/10.1109/28.585863
7. Hewitt, D., et al.: An experimental assessment of the impact of high dv/dt SiC converters on insulation lifetime of electrical machines. In: IEEE Energy Conversion Congress and Exposition (ECCE), Detroit, Mi, USA (2022)

8. Skibinski, G., et al.: Reflected wave modeling techniques for PWM AC motor drives. In: APEC '98 Thirteenth Annual Applied Power Electronics Conference and Exposition, Anaheim, CA, USA (1998)
9. Melfi, M., et al.: Effect of surge voltage risetime on the insulation of low-voltage machines fed by PWM converters. IEEE Trans. Ind. Appl. 34(4), 766–775 (1998). https://doi.org/10.1109/28.703971
10. Sundeep, S., et al.: Antiresonance phenomenon and peak voltage stress within PWM inverter fed stator winding. IEEE Trans. Ind. Electron. 68(12), 11826–11836 (2021). https://doi.org/10.1109/tie.2020.3048286
11. Sundeep, S., Wang, J., Griffo, A.: Holistic modeling of high-frequency behavior of inverter-fed machine winding, considering mutual couplings in time domain. IEEE Trans. Ind. Appl. 57(6), 6044–6057 (2021). https://doi.org/10.1109/tia.2021.3105954
12. Peng, H., et al.: High-frequency modeling of permanent magnet synchronous machines using grey box models. IEEE Transactions on Transportation Electrification, 1 (2024). https://doi.org/10.1109/tte.2024.3363511
13. Ruiz-Sarrio, J.E., et al.: Impedance modeling oriented toward the early prediction of high-frequency response for permanent magnet synchronous machines. IEEE Trans. Ind. Electron. 70(5), 4548–4557 (2023). https://doi.org/10.1109/tie.2022.3189075
14. Zhou, W., Diab, M.S., Yuan, X.: Impact of parasitics and load current on the switching transient time and motor terminal overvoltage in SiC-based drives. In: IEEE Energy Conversion Congress and Exposition (ECCE). Detroit (2020)
15. Nise, N.S.: Control System Engineering, 7th ed. John Wiley & Sons, Inc., Hoboken, NJ (2015)
16. Hewitt, D.A., et al.: High frequency modeling of electric machines using finite element analysis derived data. IEEE Trans. Ind. Electron. 71(2), 1432–1442 (2024). https://doi.org/10.1109/tie.2023.3260357
17. Xie, Y., et al.: Investigation of surge voltage propagation in inverter-driven electric machine windings. IEEE Trans. Ind. Electron. 70(10), 9811–9822 (2023). https://doi.org/10.1109/tie.2022.3220863
18. Yang, H., et al.: Comparative study of motor topologies for electric power steering system. In: IEEE Workshop on Electrical Machines Design, Control and Diagnosis (WEMDCD). Modena (2021)
19. EL-Refaie, A.M.: Fractional-slot concentrated-windings synchronous permanent magnet machines: opportunities and challenges. IEEE Trans. Ind. Electron. 57(1), 107–121 (2010). https://doi.org/10.1109/tie.2009.2030211
20. Ishak, D., Zhu, Z.Q., Howe, D.: Comparison of PM brushless motors, having either all teeth or alternate teeth wound. IEEE Trans. Energy Convers. 21(1), 95–103 (2006). https://doi.org/10.1109/tec.2005.853765
21. Jouanne, A.v., et al.: Filtering techniques to minimize the effect of long motor leads on PWM inverter fed AC motor drive systems. In: IEEE Industry Applications Conference Thirtieth IAS Annual Meeting. Orlando (1995)
22. Moreira, A.F., et al.: Filter networks for long cable drives and their influence on motor voltage distribution and common-mode currents. IEEE Trans. Ind. Electron. 52(2), 515–522 (2005). https://doi.org/10.1109/tie.2005.844237
23. Mishra, P., Maheshwari, R.: Design, analysis, and impacts of sinusoidal LC filter on pulsewidth modulated inverter fed-induction motor drive. IEEE Trans. Ind. Electron. 67(4), 2678–2688 (2019). https://doi.org/10.1109/tie.2019.2913824

How to cite this article: Hewitt, D.A., et al.: Impact of close proximity pulse width modulation switching events on electric machine terminal voltages. IET Electr. Power Appl. 1–11 (2024). https://doi.org/10.1049/elp2.12495